Ultramicroscopy 202 (2019) 100–106

Contents lists available at ScienceDirect

Ultramicroscopy

journal homepage: www.elsevier.com/locate/ultramic

A hybrid genetic-Levenberg Marquardt algorithm for automated spectrometer design optimization

Kang Hao Cheong*[,a,b], Jin Ming Koh[a]

[a] Science and Math Cluster, Singapore University of Technology and Design, 8 Somapah Road, S487372, Singapore
[b] Engineering Cluster, Singapore Institute of Technology, 10 Dover Drive, S138683, Singapore

ARTICLE INFO

Keywords:
Computational optimization
Energy analyzer
Electron optics
Genetic algorithm
Hybrid algorithm

ABSTRACT

Advancements in computational tools have driven increasingly automated, simulation-centric approaches in the design and optimization of spectroscopic electron-optical systems. These augmented methodologies accelerate the optimization process, and can yield better-performing instruments. While classical gradient-based methods had been explored, modern alternatives such as genetic algorithms have rarely been applied. In this paper, we propose a novel fully-automated hybrid optimization method for use on electron-optical systems. An adaptive switching scheme between a Levenberg–Marquardt and a genetic sub-algorithm enables the simultaneous exploitation of the computational efficiency of the former and the robustness of the latter. The hybrid algorithm is demonstrated on two test examples—the parallel cylindrical mirror analyzer, and the first-order focusing parallel magnetic sector analyzer—and is found to outperform both the Levenberg–Marquardt and genetic algorithms individually. Our work is significant as a versatile tool for parallel energy spectrometer design, and can greatly aid the development of mechanically-complex parallel energy analyzers, which are expected to be of utility to the semiconductor industry in the near future.

1. Introduction

The design and optimization of electron-optical systems for focusing performance and resolution had been accorded considerable research attention [1], but much potential remains untapped. A shift from the traditional approach of mechanically approximating known analytical fields and menial optimization to computationally-heavy, simulation-driven methodologies had been evident to date [2,3], driven by the availability of increasingly powerful computational resources. Appropriately applied, such augmented methods can accelerate the design and optimization process significantly, and yield better-performing instruments.

The recent introduction of parallel energy/mass analyzers [4–9], capable of simultaneous data acquisition over an energy range spanning orders of magnitude, further instigates the need for versatile computational tools. The design complexity and large degree-of-freedom in these instruments, and the inherent nonlinearities in field and focusing behaviour, render manual tuning largely infeasible. To be effective, computational optimization algorithms must be efficient in exploring a high-dimensional search space, and must be robust to instrument geometry, starting configuration, and solution stagnation.

Existing optimization algorithms can be broadly classified into two groups: gradient-based classical methods, such as gradient descent [10,11], pseudo-second-derivative (PSD) [12], and the Levenberg–Marquardt algorithm [13–16], and comparatively modern non-gradient based ones, such as genetic algorithms [17–19], simulated annealing [20,21], and particle swarm optimization [22–24]. The latter category offers great robustness in finding the global minimum, as opposed to gradient-based methods, which typically converge towards local minima; but such is at considerably greater computational cost, especially in high-dimensional search spaces. It will be greatly advantageous to have an optimization algorithm that is both efficient and robust to local minima entrapment—this is the focus of the current paper.

A recent paper has investigated the use of a Levenberg–Marquardt algorithm for the optimization of parallel energy spectrometer design [14]; however, genetic algorithms have not been much utilized to date. It is of immense interest to compare these two optimization methods on parallel energy spectrometer optimization. In this paper, we propose an original and novel hybrid optimization method for use on electron-optical systems. An adaptive switching process between a Levenberg–Marquardt and a genetic sub-algorithm enables the simultaneous exploitation of the computational efficiency of the former and the robustness of the latter, and also aids in recovery from solution

* Corresponding author at: Science and Math Cluster, Singapore University of Technology and Design (SUTD), 8 Somapah Road, S487372, Singapore.
E-mail address: kanghao_cheong@sutd.edu.sg (K.H. Cheong).

https://doi.org/10.1016/j.ultramic.2019.03.004
Received 4 November 2018; Received in revised form 6 January 2019; Accepted 14 March 2019
Available online 15 March 2019
0304-3991/

stagnation. We demonstrate the proposed algorithm on the parallel cylindrical mirror analyzer [25,26] and the first-order focusing parallel magnetic sector analyzer [27], indeed observing superior optimization performance from the hybrid algorithm in comparison with the Levenberg–Marquardt and genetic algorithms individually. The proposed algorithm is implemented in *Java* for general applicability, and can be coupled to any simulation software, including *COMSOL Multiphysics* and *Lorentz 2/3-EM*, through linking Application Programming Interfaces (APIs) or user interface manipulation libraries.

2. Materials & methods

In this section, we describe the genetic and Levenberg–Marquardt optimization algorithms (Sections 2.1 and 2.2), followed by the construction of the hybrid algorithm from these preliminaries (Section 2.3) incorporating an adaptive switching scheme.

Throughout this paper, the parameter vector of an analyzer configuration is denoted $\mathbf{p}$, whose m entries may represent geometric quantities or electrode/magnetic excitation potentials. The relative energy resolution is denoted $E(v)$ where v is the energy, and is computed via a direct charged-particle tracing on a numerical field solution (Section 2.4). The mean relative energy resolution across the energy range of the instrument is denoted $\overline{E}$.

2.1. Genetic algorithm

Genetic algorithms mimic the process of natural selection as an optimization protocol [17,18], and are a class of well-established evolutionary methodologies suited for solving minimization or maximization problems, even when the search space is large and topologically complex [28,29]. Many aspects of biological evolution, including the mechanisms of mating, reproduction, and mutation, and the abstracted concepts of survival fitness and selection pressure, are modelled within the algorithm. This yields robust methods capable of finding the global extremum; but despite their advantages, genetic algorithms have rarely been applied to charged-particle optical systems [19].

Broadly, genetic algorithms maintain a population of many individuals, each carrying a genotype representing a solution to the problem of interest. The suitability of each solution is evaluated via a fitness function. The population is evolved over numerous iterations to give rise to a highly-fit genotype. In each iteration, individuals are chosen on a survival-of-the-fittest basis to mate; offspring are then created through genetic recombination, in which portions of the parent genomes are exchanged in manners inspired by what occurs in nature. The population is then subjected to probabilistic mutations, wherein portions of their genomes are randomized, and the evolution cycle repeats. A flowchart of this generalized overview is presented in Fig. 1.

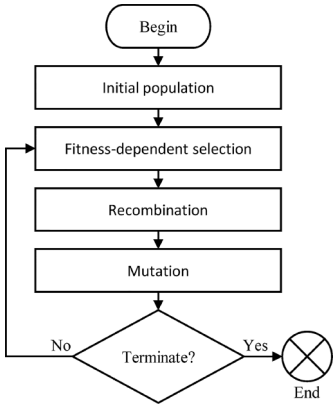

Fig. 1. Generic overview of a simplistic genetic algorithm, showing the key processes that occur in the evolution of the population.

In our implementation, each individual in the population $\mathcal{I} \in \mathcal{P}$ represent a specific configuration of the energy analyzer design, and the genotype $\mathbf{g}(\mathcal{I})$ is accordingly a real-valued vector with $g_i(\mathcal{I}) \in [-1, 1]$. The corresponding parameter vector is obtained via a transformation $p_i = \kappa_i^+ g_i H(g_i) + \kappa_i^- g_i [1 - H(g_i)]$, where H is the Heaviside step function and $\kappa_i^\pm$ are scale factors that reflect the explorable range of parameter values. Each individual is also characterized by a fitness value $f(\mathcal{I}) \equiv \overline{E}$, set to the mean relative energy resolution, whose minimization is desired.

Ideally, the scale factors $\kappa_i^\pm$ should be chosen to avoid non-workable configurations; but such accurate *a priori* restrictions are not always feasible, especially when the instrument geometry is complex. Individuals are therefore automatically tested and categorized to be legal or illegal—the latter being non-workable solutions, for instance due to geometric obstructions in the electron paths, or electron trajectories that miss the detector. The population $\mathcal{P}$ is subdivided accordingly into pools $\mathcal{P}_+$ and $\mathcal{P}_-$ containing legal and illegal individuals respectively.

To begin, the algorithm initializes the population to size n, with an individual reflecting the specified starting configuration and $(n - 1)$ individuals carrying randomly mutated genomes of the first (Fig. 2). This process seeds solutions scattered widely across the parameter space, thereby improving the odds of finding a global optimum in later iterations—this is analogous to the benefits of preserving genetic diversity in biological systems.

At each iteration, n_s individuals are selected for breeding from $\mathcal{P}_+$ through a roulette-wheel scheme favoring fitter individuals, and all remaining individuals are discarded. These n_s individuals give rise to children in a pair-wise manner through genetic recombination. Here we consider a parallelized scheme consisting of three recombination processes—one-point crossover, uniform crossover, and linear-combination crossover—each with an associated probability of occurrence. This breeding process restores the population size to n. Lastly, the occurrence of random and Gaussian stochastic point-mutations is emulated. Table 1 presents the details of these genetic operations, with U and N denoting the continuous uniform and Gaussian distributions, and U^* denoting the discrete uniform distribution of integral values.

Parallel to this evolution pipeline is an elitist selection of n_e fittest individuals, which are injected directly from one iteration to the next without evolutionary modification. This protects the best-known solutions from degradation, and allows for relatively high mutation rates to assist in exploring the solution landscape without hindering convergence performance.

2.2. Levenberg–Marquardt algorithm

The theoretical basis of the Levenberg–Marquardt algorithm is well-known [13,14] and will not be discussed at length in this paper. In the present implementation (Fig. 2), the merit function $\varphi = \mathbf{E}^2$ is taken to be the sum of squared relative energy resolutions evaluated over a set of sampling energies.

At each iteration, the Jacobian matrix $J_{ij} = \partial E_i / \partial p_j$ is computed using the linear approximation $\partial E_i / \partial p_j \approx [E_i(p_1, \ldots, p_j + \Delta p_j, \ldots, p_m) - E_i(p_1, \ldots, p_j, \ldots, p_m)] / \Delta p_j$ where $\Delta p_j \sim 10^{-2} p_j$ is small. The change vector for $\mathbf{p}$ can then be computed as $\boldsymbol{\delta} = -(\mathbf{J}^T\mathbf{J} + \Lambda\mathbf{I})^{-1}\mathbf{J}^T\mathbf{p}$ where Λ is the damping factor, thereby propagating $\mathbf{p}$ into the next iteration. As there is, in general, no systematic method for determining optimal Λ values *a priori* to yield efficient convergence, the algorithm oscillatorily trials a number of distinct Λ values in an attempt to find an adequate improvement in the solution. This process is controlled by a convergence constant $\xi \in (0, 1)$, such that trials are attempted until the current performance metric M has decreased sufficiently relative to that of the previous iteration M^-, in particular $M < \xi M^-$. Here we take $M \equiv \overline{E}$.

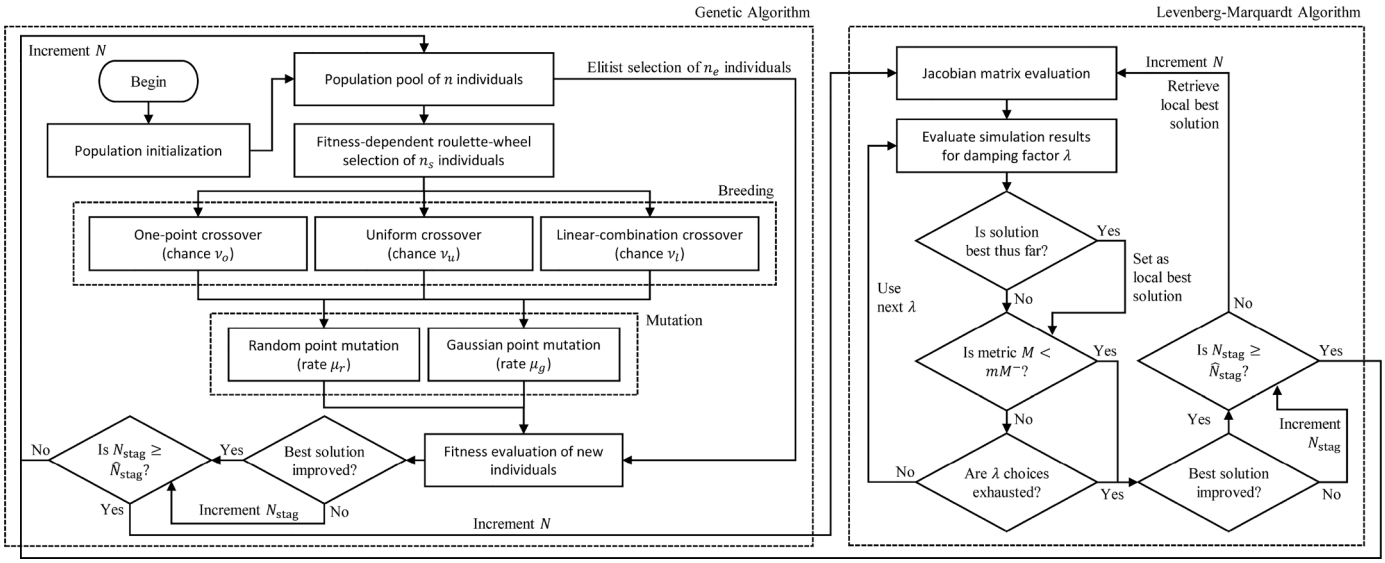

Fig. 2. Flowchart illustrating the proposed hybrid optimization method. An adaptive switching process between a Levenberg–Marquardt and a genetic sub-algorithm is implemented based on a stagnation detection scheme.

2.3. Hybridized compound algorithm

The genetic and Levenberg–Marquardt algorithms are of distinct merits and shortfalls. The maintenance of a large population pool and the stage-wise modelling of fitness-dependent selection, breeding, and mutation processes in the genetic algorithm demand a large number of merit function (fitness) evaluations per iteration. In the current context, these evaluations entail the numerical solving of the field distribution followed by charged-particle tracing through numerical integration, and are therefore computationally expensive. The Levenberg–Marquardt algorithm expends fewer evaluations per iteration, and is more efficient in this regard. In contrast, the Levenberg–Marquardt algorithm, similar to most other gradient-based methods, is inherently a local-minima search, whereas genetic algorithms are typically sufficiently robust to approach the global minimum. Better asymptotic optimization performance is therefore expected from genetic algorithms, albeit at greater computational cost.

The problem of solution stagnation is also prominent [14]. The Levenberg–Marquardt and genetic algorithms are both susceptible to solution stagnation, the former due largely to numerical noise-induced false local minima on the merit function landscape, and the latter inherent in the highly stochastic nature of the modelled evolutionary processes. The greatly nonlinear optical behaviour of complex energy analyzers in response to geometry and electrode modifications also hinders convergence.

To exploit the merits of both algorithms, and to simultaneously address solution stagnation, we propose a hybrid method (Fig. 2). The method begins with optimization via genetic algorithm, and each consecutive instance of stagnation N_{stag} is tracked. When some maximum limit $\hat{N}_{stag}$ is reached, the method transitions into the Levenberg–Marquardt algorithm, with the best-known configuration from the genetic phase used as the starting configuration. Similarly, when excessive stagnation is detected in the Levenberg–Marquardt phase, the method switches back to the genetic algorithm, with the best-known solution carried over. This switching process continues until some iteration limit $\hat{N}$ is reached, or when a specified target metric $\hat{M}$, for instance a target mean relative energy resolution, is reached.

2.4. Software implementation details

The proposed genetic algorithm, Levenberg–Marquardt algorithm, and hybrid algorithm are implemented in *Java* for general applicability, and is coupled to *COMSOL Multiphysics* via the *COMSOL API for Java*. Other simulation softwares can be used in place of *COMSOL* through linking APIs or user interface manipulation libraries. The program is configured to automatically load pre-constructed simulation files containing the CAD models and specifications of the energy analyzers; native construction of the simulation models in *Java* is also possible. In our implementation, the field distributions are computed via finite-element method, and the trajectories of the charged particles are computed via a fifth-order Runge-Kutta numerical integration.

3. Results

We emulate the general design specifications of the parallel

Table 1
Details of genetic operations.

Type	Operation	Details
Selection	Roulette-Wheel Selection	Individuals $\mathcal{I} \in \mathcal{P}$ are chosen randomly with probability $f(\mathcal{I})^{-1} / \sum_{\mathcal{J} \in \mathcal{P}} f(\mathcal{J})^{-1}$ for a total of n_s chosen individuals.
Recombination	One-Point Crossover	Genomes of offspring $\mathbf{g}^{\pm}$ are constructed from genomes of parents $\hat{\mathbf{g}}^{\pm}$ as: $g_i^{\pm} = \begin{cases} \hat{g}_i^{\pm}, & i < z \\ \hat{g}_i^{\mp}, & i \geq z \end{cases}$ where $z \sim U^*(1, m+1)$.
	Uniform Crossover	Construction of offspring genomes is: $g_i^{\pm} = z_i \hat{g}_i^{\pm} + (1 - z_i)\hat{g}_i^{\mp}$ where $z_i \sim U^*(0, 1)$.
	Linear-Combination Crossover	Construction of offspring genomes is: $g_i^{\pm} = \lambda \hat{g}_i^{\pm} + (1 - \lambda)\hat{g}_i^{\mp}$ where $\lambda \sim U(0, 1)$.
Mutation	Random Point Mutation	Genome $\mathbf{g}$ of each individual $\mathcal{I} \in \mathcal{P}$ is modified with probability μ_r as $g_i = x$, $i \sim U^*(1, m)$, $x \sim U(-1, 1)$.
	Gaussian Point Mutation	Genome $\mathbf{g}$ of each individual $\mathcal{I} \in \mathcal{P}$ is modified with probability μ_g as $g_i = \max(\min(x, 1), -1)$, $i \sim U^*(1, m)$, $x \sim N(g_i, 0.3)$.

cylindrical mirror analyzer (Section 3.1) and the first-order focusing parallel magnetic sector analyzer (Section 3.2) in *COMSOL Multiphysics* as way of example, on which we demonstrate our proposed hybrid algorithm. Performance comparisons using the proposed hybrid algorithm are presented in Sections 3.1 and 3.2 for the two instruments respectively, with the number of fitness evaluations N_{eval} as a platform-independent metric for computational time.

3.1. Parallel cylindrical mirror analyzer

The parallel cylindrical mirror analyzer (PCMA) [25,26] is an evolution of the canonical cylindrical mirror analyzer (CMA) design [30] to support parallel data acquisition across the majority of the Auger electron energy range (125 eV–3000 eV). The instrument consists of two concentric cylinders with an axially-placed source, and can function in the axis-to-cylinder, axis-to-axis, and axis-to-disk modes. The axis-to-cylinder mode is used for the current example.

The original design entails a linearly-varying potential on the outer cylinder—but this does not necessarily represent an optimal configuration of this design. As an improvement, we segment the outer cylinder into 12 individually-tunable electrodes, separated from one another via insulating rings. A schematic of this revised design is presented in Fig. 3. A starting parameter configuration of electrode potentials $V_1 = -3825.0\,\text{V}$, $V_2 = -3423.1\,\text{V}$, $V_3 = -3021.2\,\text{V}$, $V_4 = -2619.3\,\text{V}$, $V_5 = -2217.4\,\text{V}$, $V_6 = -1815.5\,\text{V}$, $V_7 = -1413.6\,\text{V}$, $V_8 = -1011.7\,\text{V}$, $V_9 = -609.8\,\text{V}$, $V_{10} = -207.9\,\text{V}$, $V_{11} = 194.02\,\text{V}$, $V_{12} = 595.93\,\text{V}$, source position $z_s = -1.85R_1$ and central pass angle $\theta = 0.472\,\text{rad}$ was taken, with length scale $R_1 = 1\,\text{mm}$. These initial electrode potentials were obtained from the $V = -(250\ln 4)z$ linearly-varying distribution proposed in the original design, as evaluated on the centroids of the segmented electrodes.

Fig. 4(a) presents optimization results yielded by the hybrid, genetic, and Levenberg–Marquardt algorithms, for a polar angular spread of $\Delta\theta = \pm 16\,\text{mrad}$, consistent with the original specifications. As merit function evaluations occupy the vast majority of computational resources, the number of evaluations N_{eval} can be taken as directly proportional to computational time, thereby giving a measure of the convergence speed of the algorithms. The superior performance of the hybrid algorithm is evident. In particular, the hybrid algorithm on average yields 11.9% and 6.4% better mean relative energy resolution than the Levenberg–Marquardt and genetic algorithms respectively at $N_{\text{eval}} = 500$; similar figures of 12.3% and 5.3% respectively are observed for $N_{\text{eval}} = 1000$. Fig. 4(b) presents a comparison of the initial and optimized relative energy resolution landscapes, illustrating the improved focusing performance across the energy range of the instrument.

3.2. First-order focusing parallel magnetic sector analyzer

The first-order focusing parallel magnetic sector analyzer [27] is a cuboid-shaped instrument operating in the Auger electron energy range, with three pairs of magnets mounted internally as focusing elements. The drastically different geometry of the device, and the magnetostatic operating principle in place of electrostatics, motivates the use of this analyzer instrument as a meaningful second demonstration example. Fig. 5 presents a schematic of the design. The compactness of the analyzer allows an array to be formed in the azimuthal direction to increase transmission, and physical prototypes have indeed been built [27].

The original design was derived by emulating a known Gaussian analytical field; here, we apply the proposed hybrid algorithm for an automated optimization. For simplicity, a scalar magnetic potential formulation is adopted. A starting configuration of magnetic excitation potentials $\varphi_1 = 9\,\text{A}\,\text{T}$, $\varphi_2 = 25\,\text{A}\,\text{T}$, $\varphi_3 = 90\,\text{A}\,\text{T}$, source position $y_s = 18\,\text{mm}$ and central pass angle $\theta = 0\,\text{rad}$ was taken, consistent with the original specifications. Fig. 6(a) presents optimization results yielded by the hybrid, genetic, and Levenberg–Marquardt algorithms, for a polar angular spread of $\Delta\theta = \pm 25\,\text{mrad}$; and Fig. 6(b) presents a comparison of the initial and optimized relative energy resolution landscapes. The superior performance of the hybrid algorithm is once again evident, yielding 5.5% and 5.2% better mean relative energy resolution than the Levenberg–Marquardt and genetic algorithms respectively at $N_{\text{eval}} = 900$. Note that the original design had already been manually optimized [27], and its design can be assumed to be optimal to a reasonable extent.

4. Discussion

The combination of the precursory Levenberg–Marquardt and genetic algorithms into an adaptive switching hybridized algorithm yields better convergence performance than either individually. This fusion between evolutionary and gradient-based methods, shown here to be very successful in computational spectrometer optimization, is also broadly applicable to other problems where solution stagnation is a major challenge. The simultaneous robustness and efficiency of the hybrid algorithm is expected to be of interest to a broad variety of fields besides electron-optical engineering.

The construction of the presented hybrid algorithm was originally motivated by the game-theoretic Parrondo's paradox, in which a winning outcome is achieved by playing two losing games in a deterministic or stochastic order [14,31–33]. In the canonical paradox, a diffusive probabilistic *Game A* is played alongside a ratcheting *Game B* in an intercalated fashion; the perturbations introduced by the former

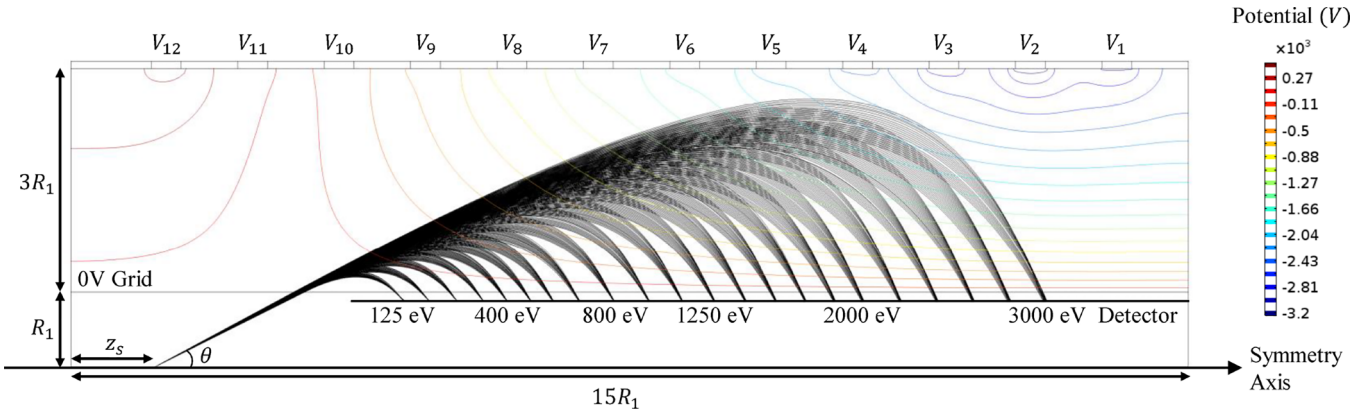

Fig. 3. Schematic of the parallel cylindrical mirror analyzer with segmented electrodes. A length scale of $R_1 = 1\,\text{mm}$ is taken. Computed electric potential contours are shown, alongside simulated electron trajectories for $\Delta\theta = \pm 16\,\text{mrad}$. The presented configuration is an optimized solution found via our hybrid algorithm, also depicted in Fig. 4(b).

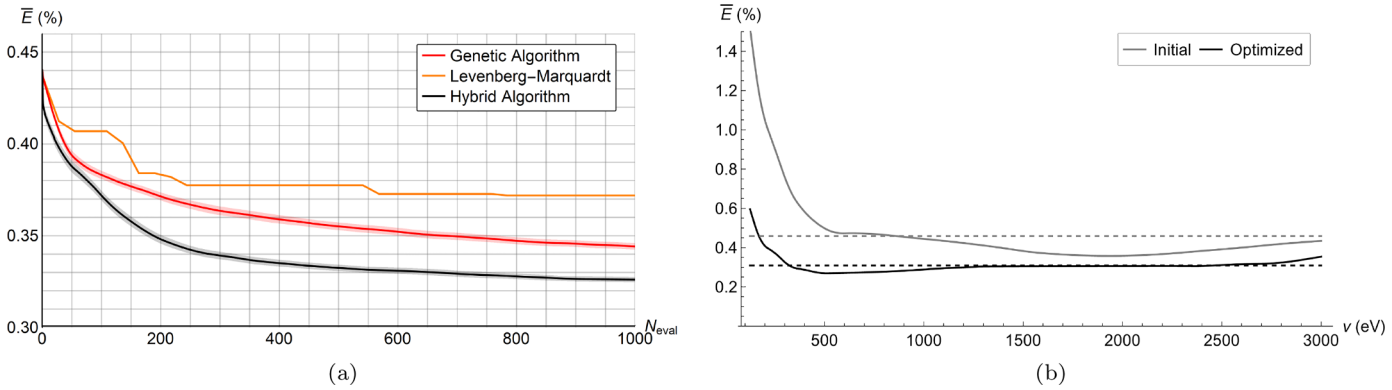

Fig. 4. (a) Plot of best-known mean relative energy resolution against merit function evaluation count, comparing the genetic, Levenberg–Marquardt, and hybrid algorithms. Results for the inherently stochastic genetic and hybrid algorithms were averaged over 100 repetitions (solid line), with 95% confidence intervals in colored shading. (b) A comparison of the initial and optimized relative energy resolution landscapes as yielded from the hybrid algorithm. The optimized instrument is of mean relative energy resolution $\overline{E} = 0.309\%$. Parameters used are $n = 20$, $n_s = 10$, $n_e = 2$, $[v_o \;\; v_u \;\; v_l] = [0.4 \;\; 0.2 \;\; 0.4]$, $[\mu_r \;\; \mu_g] = [0.3 \;\; 0.1]$, and $\hat{N}_{stag} = 3$. (For interpretation of the references to color in this figure legend, the reader is referred to the web version of this article.)

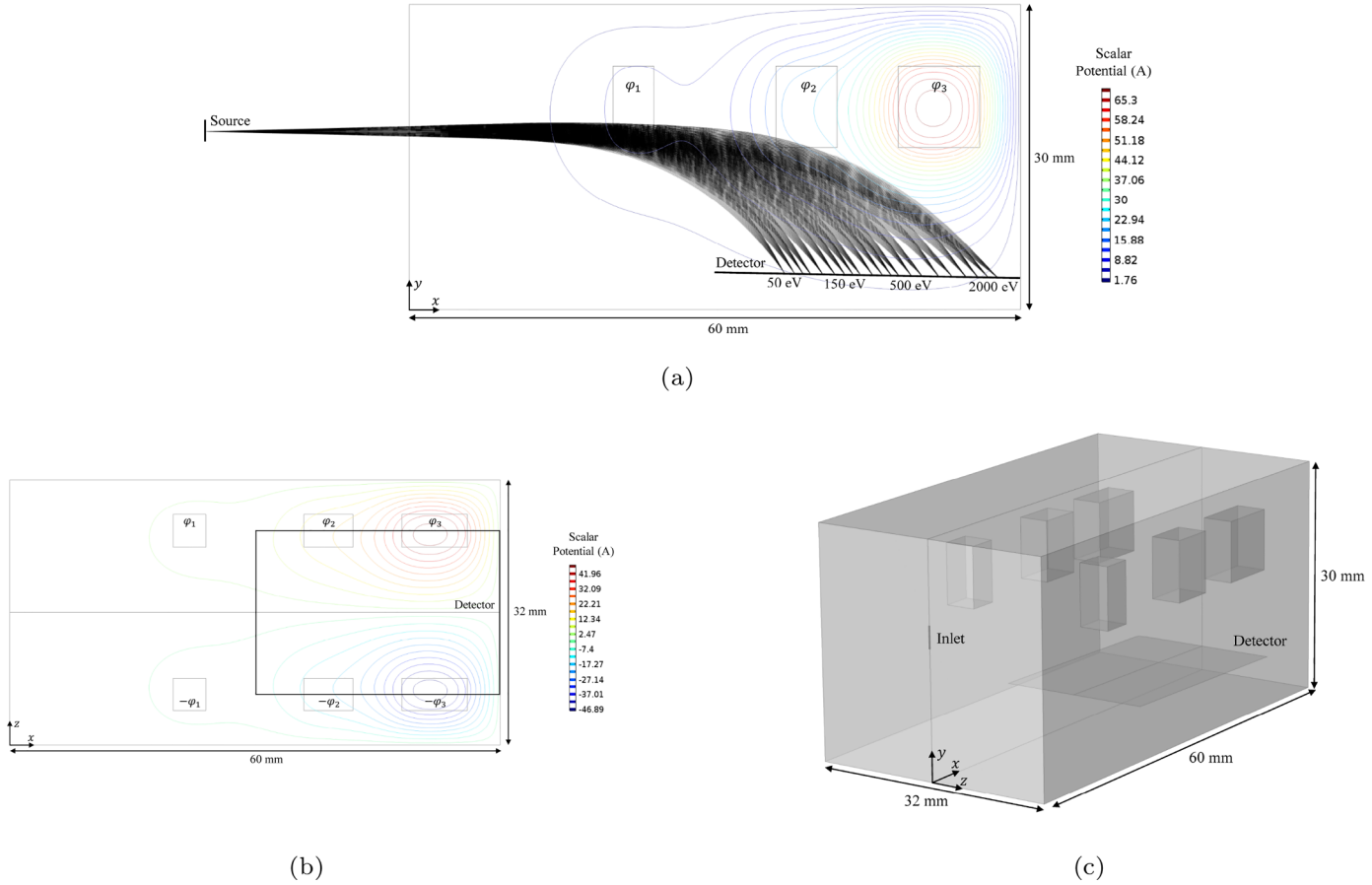

Fig. 5. Schematics of the first-order focusing parallel magnetic sector analyzer. In (a), a side view is presented, showing the three pairs of magnets. Computed magnetic scalar potential contours are shown, alongside simulated electron trajectories for $\Delta\theta = \pm 25$ mrad. The presented configuration is an optimized solution found via the hybrid algorithm, also depicted in Fig. 6(b). In (b), a top view is shown; and in (c), a three-dimensional rendering is presented.

enables a sustained exploitation of asymmetry in the latter, yielding enhanced outcomes. Here, in the hybrid algorithm, the genetic algorithm phase seeds considerable diversity in the solution search space, by virtue of the mutatory and recombination processes—this is analogous to the diffusive *Game A*. On the other hand, the Levenberg–Marquardt algorithm forgoes diversity in exchange for the speedy optimization of a single starting solution, and can be compared with the ratcheting *Game B*. The result, when adaptively alternating between these two processes, is that the solution space is repeatedly explored and promising trials efficiently refined, thereby overcoming the local-minima limitation of the Levenberg–Marquardt algorithm whilst preserving reasonable speed. This robustness of the hybrid algorithm to local-minima entrapment helps it outperform the individual sub-algorithms, as observed in the presented results (Figs. 4 and 6). As the sub-algorithms individually achieves convergence, albeit sub-optimal ones, the current study suggests an emergence of the *weak* Parrondo effect [34], as opposed to the *strong* effect. In the former, two strategies are combined to produce an outcome that is better than

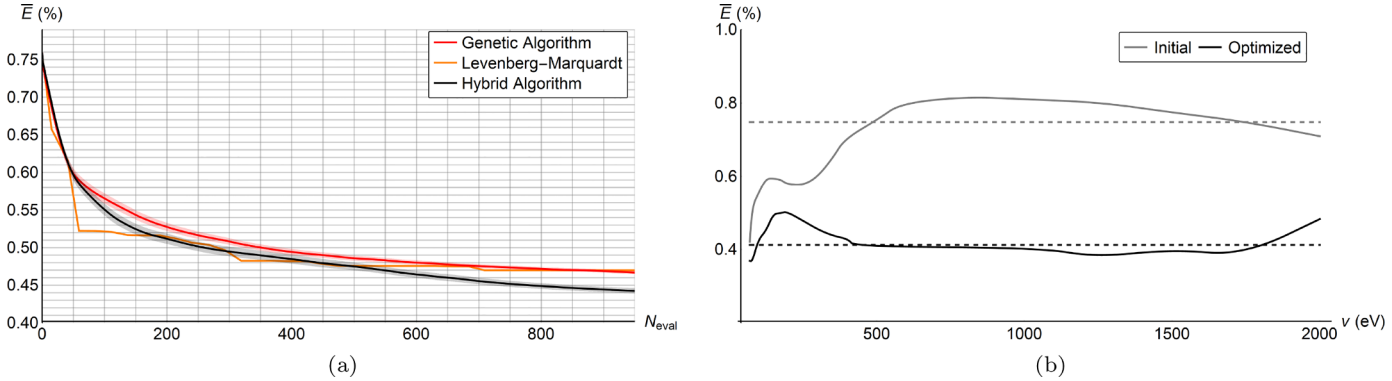

Fig. 6. (a) Plot of best-known mean relative energy resolution against merit function evaluation count, comparing the genetic, Levenberg–Marquardt, and hybrid algorithms. Results for the inherently stochastic genetic and hybrid algorithms were averaged over 100 repetitions (solid line), with 95% confidence intervals in colored shading. (b) A comparison of the initial and optimized relative energy resolution landscapes as yielded from the hybrid algorithm. The optimized instrument is of mean relative energy resolution $\overline{E} = 0.412\%$. Parameters used are $n = 20$, $n_s = 10$, $n_e = 2$, $[v_o \;\; v_u \;\; v_l] = [0.4 \;\; 0.2 \;\; 0.4]$, $[\mu_r \;\; \mu_g] = [0.3 \;\; 0.1]$, and $\hat{N}_{stag} = 3$. (For interpretation of the references to color in this figure legend, the reader is referred to the web version of this article.)

otherwise possible with each strategy individually. It remains to be seen whether the strong effect, where sub-strategies entirely fail to converge whilst the mixed strategy succeeds, can manifest in a practical engineering context.

It is also notable that the proposed algorithm can, in principle, be coupled to any simulation software, through the use of linking APIs or user interface manipulation libraries. To date, only a limited range of commercial simulation software offer native optimization functionalities suitable for electron-optical systems. Importantly, the algorithm implementation here offers an add-on automated optimization capability to software that is specialized for electron-optical systems, and can potentially be of great utility in the design and development of spectroscopic instruments of complex design.

5. Conclusion

The current study has presented a novel hybrid optimization algorithm, implementing an adaptive switching scheme between a constituent Levenberg–Marquardt and a genetic algorithm. Such an approach exploits the global minimum search capabilities of the latter alongside the computational speed of the former, creating a best-of-both-worlds middle ground that is robust and efficient. The proposed hybrid algorithm has been demonstrated on the parallel cylindrical mirror analyzer and the first-order focusing parallel magnetic sector analyzer as test examples, and the optimization performance yielded was shown to be significantly superior to both the Levenberg–Marquardt and the genetic algorithm individually. The presented algorithm can be coupled to various simulation software through APIs or linking libraries, and is applicable to a wide variety of optimization problems.

As the semiconductor technology roadmap predicts shrinking node sizes, standard defect inspection techniques will no longer be sufficient. Our algorithm can be used to develop improved parallel energy spectrometer attachments for the scanning electron microscope, so that quantitative elemental analysis can be mapped with high image resolution on the nano-scale. It can also be used to optimize parallel mass spectrometer design for use as an add-on attachment on focused ion beam instruments. Recent studies have indicated that improvements in energy analyzer focusing performance can be achieved through electrode segmentation [35,36], enhancing resolution at the cost of increased mechanical complexity. An effective automated optimization tool such as that presented here will be of great practical value in the development of these high-complexity electron-optical instruments.

6. Code availability

The optimization toolkit can be downloaded from Open Science Framework (OSF) at https://goo.gl/7fMdWp.

Acknowledgement

Kang Hao Cheong acknowledges the support of SUTD Start-up Research Grant (SRG SCI 2019 142).

References

[1] A. Khursheed, Energy analyzer attachments for the scanning electron microscope, Microsc. Microanal. 21 (S4) (2015) 130–135.
[2] Z. Aiming, A. Khursheed, Accurate ray tracing through finite element solved potential distributions in charged particle optics, Proc. SPIE, 3777 (1999).
[3] H.C. Chu, E. Munro, Computerized optimization of electron-beam lithography systems, J. Vac. Sci. Technol. 19 (4) (1981) 1053–1057.
[4] D. Cubric, A.D. Fanis, I. Konishi, S. Kumashiro, Parallel acquisition electrostatic electron energy analyzers for high throughput nano-analysis, Nucl. Instrum. Methods Phys. Res. Sect. A 645 (1) (2011) 227–233.
[5] K.H. Cheong, W. Han, A. Khursheed, K. Nelliyan, A parallel radial mirror energy analyzer attachment for the scanning electron microscope, Microsc. Microanal. 21 (S4) (2015) 142–147.
[6] K.H. Cheong, A. Khursheed, A parallel magnetic sector mass analyzer design, Nucl. Instrum. Methods Phys. Res. Sect. A 645 (1) (2011) 221–226.
[7] A. Khursheed, K.H. Cheong, H.Q. Hoang, Design of a parallel mass spectrometer for focused ion beam columns, J. Vac. Sci. Technol. B Nanotechnol. Microelectron. 28 (6) (2010) C6F10–C6F14.
[8] A. Khursheed, H.Q. Hoang, A. Srinivasan, A wide-range parallel radial mirror analyzer for scanning electron/ion microscopes, J. Electron Spectros. Relat. Phenomena 184 (11) (2012) 525–532.
[9] A. Khursheed, Design of a parallel magnetic box energy analyzer attachment for electron microscopes, J. Electron Spectros. Relat. Phenomena 184 (1) (2011) 57–61.
[10] A. Shapiro, Y. Wardi, Convergence analysis of gradient descent stochastic algorithms, J Optim Theory Appl 91 (2) (1996) 439–454.
[11] M. Avriel, Nonlinear Programming: Analysis and Methods, Courier Corporation, 2003.
[12] D.C. Dilworth, Pseudo-second-derivative matrix and its application to automatic lens design, Appl. Opt. 17 (21) (1978) 3372–3375.
[13] D.W. Marquardt, An algorithm for least-squares estimation of nonlinear parameters, J. Soc. Indus. Appl.Math. 11 (2) (1963) 431–441.
[14] J.M. Koh, K.H. Cheong, Automated electron-optical system optimization through switching Levenberg–Marquardt algorithms, J. Electron Spectros. Relat. Phenomena 227 (2018) 31–39.
[15] M. Nunn, C.G. Wynne, Lens designing by electronic digital computer: Ii, Proc. Phys. Soc. 74 (3) (1959) 316.
[16] K. Levenberg, A method for the solution of certain non-linear problems in least squares, Q. Appl. Math. 2 (2) (1944) 164–168.
[17] A. Brunetti, A fast and precise genetic algorithm for a non-linear fitting problem, Comput. Phys. Commun. 124 (2) (2000) 204–211.
[18] D. Vasiljevic, Classical and Evolutionary Algorithms in the Optimization of Optical

Systems, Springer Science & Business Media, 2012.
[19] C. Gu, M.Q. Wu, L. Shan, G. Lin, Application of genetic algorithms to the optimization design of electron optical system, Proc. SPIE 4510 (2001), https://doi.org/10.1117/12.451273.
[20] H. Szu, R. Hartley, Fast simulated annealing, Phys. Lett. A 122 (3) (1987) 157–162.
[21] S. Kirkpatrick, Optimization by simulated annealing: quantitative studies, J. Stat. Phys. 34 (5) (1984) 975–986.
[22] E. Bonabeau, M. Dorigo, G. Theraulaz, Inspiration for optimization from social insect behaviour, Nature 406 (2000) 39.
[23] C. Gollub, R. de Vivie-Riedle, Modified ant-colony-optimization algorithm as an alternative to genetic algorithms, Phys. Rev. A 79 (2009) 021401.
[24] R. Poli, J. Kennedy, T. Blackwell, Particle swarm optimization, Swarm Intell. 1 (1) (2007) 33–57.
[25] F.H. Read, The parallel cylindrical mirror electron energy analyzer, Rev. Sci. Instrum. 73 (3) (2002) 1129–1139.
[26] F. Read, D. Cubric, S. Kumashiro, A. Walker, The parallel cylindrical mirror analyzer: axis-to-axis configuration, Nucl. Instrum. Methods Phys. Res. Sect. A 519 (1) (2004) 338–344.
[27] A. Khursheed, K. Nelliyan, F. Chao, First-order focusing parallel electron energy magnetic sector analyzer designs, Nucl. Instrum. Methods Phys. Res. Sect. A 645 (1) (2011) 248–252.
[28] J.H. Holland, Adaptation in Natural and Artificial Systems: An Introductory Analysis with Applications to Biology, Control, and Artificial Intelligence, MIT Press, 1992.
[29] D.E. Goldberg, J.H. Holland, Genetic algorithms and machine learning, Mach. Learn. 3 (2) (1988) 95–99.
[30] J.S. Risley, Design parameters for the cylindrical mirror energy analyzer, Rev. Sci. Instrum. 43 (1) (1972) 95–103.
[31] G.P. Harmer, D. Abbott, Losing strategies can win by Parrondo's paradox, Nature 402 (1999) 864–870.
[32] G.P. Harmer, D. Abbott, A review of Parrondo's paradox, Fluct. Noise Lett. 02 (2002). R71–R107
[33] D. Abbott, Asymmetry and disorder: a decade of parrondo's paradox, Fluct. Noise Lett. 09 (01) (2010) 129–156.
[34] D. Wu, K.Y. Szeto, Extended Parrondo's game and Brownian ratchets: strong and weak parrondo effect, Phys. Rev. E 89 (2014) 022142, https://doi.org/10.1103/PhysRevE.89.022142.
[35] D. Edwards, The segmented cylindrical mirror analyzer (cma), J. Electron Spectros. Relat. Phenomena 209 (2016) 46–52.
[36] D. Edwards, Improving the performance of the cylindrical mirror analyzer II: reducing the dependence of energy resolution on sample position, J. Electron Spectros. Relat. Phenomena 212 (2016) 62–73.